

Study of Proximity Lithography Simulations Using Measurements of Dissolution Rate and Calculation of the Light Intensity Distributions in the Photoresist

Yoshihisa Sensu, Mariko Isono, Atsushi Sekiguchi, Mikio Kadoi and Toshiharu Matsuzawa
Litho Tech Japan Corporation
2-6-6 Namiki, Kawaguchi, Saitama, 332-0034, Japan
sensu@ltj.co.jp

ABSTRACT

This report describes the results of a study on resist profile simulation in proximity printing, using light intensity distribution and actually measured dissolution rate values, a method that takes the gap effect into consideration (the effect of the distance between mask and wafer on the aerial image and resist profiles). We calculate the light intensity distribution with the gap effect based on the Van Cittert-Zernike theory and on the Hopkins equation as a model of light intensity distribution of proximity printing in resist film. Dissolution rate values are obtained using an apparatus to measure resist film thickness during development. The resist profile simulation is carried out using the combined data thus obtained. To verify the validity of this simulation, we use an SEM to observe resist profiles obtained from a diazonaphthoquinone (DNQ)-novolak resin positive-type resist for thick films, varying the proximity gaps using the mask aligner, which uses light in the broadband wavelengths of 350 nm to 450 nm, and compare the results with the simulation. The results of simulation and those of the SEM observation are in agreement, proving the validity of our method.

Keywords: lithography, thick film resist, dissolution rate, proximity printing, resist profile simulation, mask aligner

1. INTRODUCTION

In recent years, electronic products have advanced remarkably, becoming smaller, lighter, and more portable, at the same time offering higher performance. These advances have been enabled in large part by the application of cutting-edge semiconductor technologies, notably those related to integrated circuits and high-density packaging. In the development of high-density packaging technology for semiconductors, lithography has played an important role. Packaging techniques such as TAB (Tape Automated Bonding, involving the use of bump electrodes), COF (Chip On Film), and COG (Chip On Glass) are used in the driving components (i.e., the driver LSI) in the liquid-crystal displays used in cellular phones and personal computers. Packaging technologies have also progressed in conjunction with higher integration in semiconductors, from the wire-bonding method to the BGA (Ball Grid Array) technique to CSP (Chip Size Package, a technique employed at the chip level) and WL-CSP (Wafer Level CSP) is now in practical use [1]. As with semiconductor integrated circuits, progress in high-density packaging technologies has been enabled through the miniaturization of patterns, made possible by advances in lithography process technology. In high-density packaging, resist patterning is often carried out through the combined application of thick film resists and mask aligners. However, if the thin film resist process used for ICs is applied without modification to the thick film resist process, problems such as low resolution are likely to occur [2]. Therefore, the process must be optimized for thick film resist. This situation highlights the growing importance of thick film resist profile simulation technology that can be applied to a contact aligner.

Various methods have been proposed to refine the resist profile simulation based on the model proposed by Dill et al. (the "Dill model") [3]. The Dill model begins with the calculation of light intensity on the resist surface and carries out simulation through numerical calculation of all elements of the processes of resist exposure and development. Grindle et al. have proposed a method (the "Grindle model") in which the light intensity distribution is obtained by numerical calculation but the simulation of development is performed based on actually measured dissolution rate

values [4]. We have previously reported on the ProxSim-1 (PROXimity SIMulator) based on the Grindle model, a simulator that combines light intensity distribution on the resist surface (in proximity printing using a mask aligner) with actually measured dissolution rate values [5]. In this paper we report on the results of simulation that takes the gap effect in resist film into consideration in proximity printing [6], [7], [8], [9].

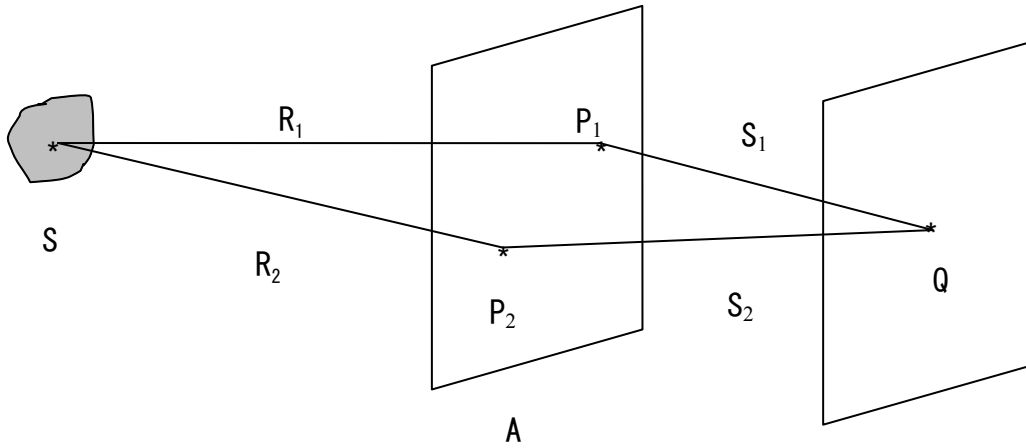
2. CALCULATION OF LIGHT INTENSITY DISTRIBUTION OF MASK ALIGNER

2.1 Light intensity distribution on resist surface

Figure 1 shows a schematic diagram of the distribution of light intensity on the resist surface. The light beams passing through the Cr (chromium) pattern slits of the mask are diffracted, with a resultant deterioration in light intensity distribution relative to the ideal. This post-pattern distribution was obtained based on the Van Cittert-Zernike theory [10], [11] and on the Hopkins equation [12].

Under the optical system of proximity printing, the relative light intensity $I(Q)$ on the resist surface Q is given by equation (1).

$$I(Q) = \iiint_A I(S) \frac{\exp [2\pi i (R_1 - R_2) / \lambda]}{R_1 R_2} \frac{\exp [2\pi i (S_1 - S_2) / \lambda]}{S_1 S_2} \Lambda_1 \Lambda_2^* dS dP_1 dP_2 \quad (1)$$



where λ is the wavelength of light, S is the light source, A is the mask surface, P_1 and P_2 are points on the mask surface, R_1 and R_2 are the distances from the light source S to the points P_1 and P_2 on the mask surface A , and S_1 and S_2 are the distances from the points P_1 and P_2 to the resist surface Q .

2.2 Determination of light intensity distribution, taking the gap effect in the resist film into consideration

Figure 2 shows a schematic diagram of the light intensity distribution in proximity printing taking the gap effect in the resist film into consideration. The gap effect in the resist film here refers to the effect of the distance between the mask and wafer (gap) on the aerial image and the resist image after development. First, resist film D is divided equally into 100 layers; the divided layers are then numbered from D_1 to D_{100} , starting from the resist surface and proceeding toward the substrate. Light intensity distributions are calculated at D_1 (on the surface) and D_{100} (at the interface between the resist and the substrate). Light intensity distribution values for the remaining film layers (from D_2 to D_{99}) are obtained through linear interpolation of the calculated values for D_1 and D_{100} . The light intensity distribution in the direction of the line width of the resist X (the horizontal direction) is obtained by dividing the resist film into 128 parts of equal width in the horizontal direction. The intensity distribution in the depth direction is calculated taking the gap effect into account at each of these 128 points.

3. MEASUREMENT OF THE DISTRIBUTION OF DISSOLUTION RATE IN THE RESIST FILM

Figure 3 shows the film thickness measurement apparatus (non-contact type) used to determine the resist dissolution rate (Model KT-22t; Foothill)[5]. Figure 4 shows the procedure used. Six samples were initially prepared by coating resist and pre-baking; each sample was then subject to 22 types of exposure, from E_1 to E_{22} (0 to 2,000 mJ/cm²). The six samples were developed for 5, 10, 15, 20, 25, and 30 minutes, respectively. After development, the thickness values of the remaining film of each sample (T_1 to T_{22}) were measured using the KT-22t to obtain the resist film thickness value against developing time for each exposure dose. Figure 5 illustrates the correlation between developing time and resist film thickness. The distribution of the dissolution rate in the resist film corresponding to each exposure dose was then obtained through differentiation of this correlation, as shown in Figure 6.

4. CALCULATION OF THE DISTRIBUTION OF DISSOLUTION RATE IN THE RESIST FILM

Figure 7 shows the procedure for calculation of the distribution of the dissolution rate in the resist film. The light intensity distribution $E(X_m, D_n)$ described above represents the aerial image intensity at resist film positions D_1 to D_{100} (Figure 7 (a)). Suppose, for example, that energy E in the resist film at a position denoted by coordinate X_m in the direction of line width and coordinate D_n in the cell of the resist film is 650 mJ/cm². Since this light intensity value of 650 mJ/cm² does not take the light absorption effect into consideration, it corresponds only to the aerial image determined by the optical system. We must therefore take both the light absorption effect and the multiple interference effect into consideration when obtaining the dissolution rate at position (X_m, D_n) . This is necessary because both of these effects will have an influence on the dissolution rate distribution. These effects can be obtained from the actually measured data. Figure 7 (b) shows the measured dissolution rate distribution in the resist film. Values on the right side of the figure represent the light exposure energy of the mask aligner. Since no data directly corresponds to a light intensity of 650 mJ/cm², the dissolution rate $R(X_m, D_n)$ corresponding to 650 mJ/cm² is determined by interpolation using the existing data for 600 mJ/cm² and 700 mJ/cm². By repeating the above-mentioned procedure for all cells shown in figure 7(c), the dissolution rate distribution in the resist film may be obtained. Thus the dissolution rate at position (X_m, D_n) can be estimated [13].

5. CALCULATION FOR DEVELOPMENT

Calculation for development is performed using the dissolution rate distribution in the resist film and the level set method [14]. The level set method is, in principle, a solution for the Eikonal equation used in optics; in this case the transfer of the resist surface created by the development involves the application of the least time principle.

6. EXPERIMENTAL RESULTS AND DISCUSSION

6.1 Experimental conditions

Figure 8 shows the experimental conditions and the process flow for the preparation of test samples. Using the LITHOTRAC (Model LARC-1000, Litho Tech Japan Corporation) for resist application and baking, diazonaphthoquinone (DNQ)-novolak resin positive-type resist for thick films (“the resist”) was applied to the silicon substrate at a thickness of 19.8 μm . The proximity baking method was used for pre-baking at 125°C for 7 minutes, which was expected to prevent the pattern deterioration caused by the generation of nitrogen bubbles due to exposure to light [15]. The samples were dehydrated in a vacuum dessicator for 1 hour and then immersed in purified water at 23°C for 30 minutes, in order to improve resolution [16]. Figure 9 shows an illustration of a mask aligner of the proximity printing type (Model UL-7000, QUINTEL). Broadband light at wavelengths from 350 nm to 450 nm was used in exposure, with the proximity gaps set to 0 μm , 1 μm , 5 μm , 10 μm , 30 μm , and 50 μm , and the collimation angle set to 1.5°. Light exposure (E_{op}) of 940 mJ/cm² (value at the i-line wavelength) was applied, using line-space pattern of 10 μm (lines to spaces ratio was 1:1). Dip development was performed at 23°C for 15 minutes

using the TMAH developing solution for thick film resist. The refractive index of the resist at the time of measurement was assumed to be 1.68, and line-space patterns of 10 μm and 4 μm were used for the inspection of resist profile.

6.2 Comparison of resist profile

Figure 10 shows the results of SEM observation and of calculations using ProxSim-1. For the proximity gap of 0 μm , the sides of the patterns have a tapered shape for pattern sizes of 10 μm and 4 μm , and bulging is observed at the surface position of the resist profiles.

For the proximity gap of 1 μm , the sides of the patterns have a tapered shape for pattern sizes of 10 μm and 4 μm , and bulging at the surface position of the resist profiles is reduced relative to the gap observed at 0 μm .

For the proximity gaps from 5 μm to 50 μm , the sides of the patterns have a tapered shape for pattern sizes of 10 μm and 4 μm . However, bulging at the surface position of the resist profiles has disappeared. Further, as the value of the proximity gap increases, the film thickness loss at the resist surface increased, resulting in a rounded profile.

These phenomena show that the results of calculations using the ProxSim-1 agreed approximately with those obtained by SEM observation, verifying in principle the accuracy of simulation using the ProxSim-1, which employs the actually measured dissolution rate and the light intensity distributions taking the gap effect in the resist film into consideration.

6.3 Light intensity and resist profile simulation

Figure 11 shows the results of calculations for light intensity at the resist surface and at the interface between the resist and the substrate for the line-spaces of 10 μm and 4 μm when the proximity gap value is varied. For the proximity gap of 0 μm , bulging at the surface of the resist profile is prominent. This phenomenon seems to be a result of the steep change in light intensity distribution between the opaque part (chromium) and the transparent part at the resist surface.

For other proximity gap values, the bulging at the top of the resist profile disappears, with greater reduction in the film thickness at the top of the resist profile as the value of the proximity gap increases, resulting in a rounded shape. Such phenomena seem to be due to decreased light intensity contrast at the resist surface.

Figure 12 shows a comparison between the results of resist profile simulations with and without consideration to the gap effect in the resist film. For proximity gaps of 0 μm and 1 μm , the bulging at the surface of the resist profile and the tapering of the sides at the bottom were well reproduced, agreeing with the results of SEM observation where the gap effect was taken into consideration. On the other hand, when the gap effect was not considered, the bulging at the surface of the resist profile and the tapering of the sides at the bottom were not reproduced. This indicates that the results of simulation agreed with the results of SEM observation when the gap effect in the resist film was taken into consideration, thus verifying the validity of the method under study.

7. CONCLUSION

The calculation model for light intensity distribution for use with the ProxSim-1 proximity printing simulator has been improved by taking the gap effect seen in resist film into consideration. ProxSim-1 simulation results agree approximately with the results of SEM observation, thus verifying the validity of this method.

REFERENCES

- [1] O. P. Lehar, M. A. Spark, S. Meyer and R. R. Dammel : "Resist rehydration during thick film processing", SPIE, 4345, pp. 463-474 (2001).
- [2] Y. Shibayama and M. Saito, : "Influence of Water on Photochemical Reaction of Positive-Type Photoresist", J. Appl. Phys., vol. 29, pp. 2152-2155 (Oct. 1990).
- [3] Dill F. H., Neureuther A. R., Ruttle J. A. and Walker E. J.: "Modeling projection Printing of Positive Photoresists" IEEE Trans. Electron Devices, ED-22, 7, pp. 456-464 (July 1975).
- [4] Yeung M. S. : "Modeling high numerical aperture optical lithography", SPIE, 922, Optical/Laser Micro lithography, pp. 149-167 (1988).
- [5] Mack C. A. : "PROLITH : a comprehensive optical lithography model", SPIE, 538, pp. 207-219 (1985).
- [6] Bernard D. A. : "Simulation of Focus Effects in Photolithography", IEEE Trans. Semiconductor

- Manufacturing, 1, 3, pp. 85-97 (Aug. 1988).
- [7] Henke W. and Czech G. : "SIMULATION OF LITHOGRAPHIC IMAGES AND RESIST PROFILES" , Elsevier Science Publishers B. V., pp. 629-633 (Nov. 1990).
 - [8] Garza C. M.,and Grindle S. O. : "Resist Characterization and Optimization Using A Development Simulation Computer Program. PROSIM" , SPIE, 631, Advances in Resist Technology and Processing 3 (1986).
 - [9] Batchelder T. and Piatt J. , : "Bakeing effect of positive photoresist" , Solid State Technology, Japanese version, pp. 55-61 (Feb. 1984).
 - [10] P. H. van Cittert : "Die wahrscheinliche Schwingungsverteilung in einer von einer Lichtquelle direct oder mittels einer Linse beleuchteten Ebene" , Physica 1, pp. 201-210 (1934).
 - [11] F. Zernike : "The Concept of Its Application to Optical Problems" , Physics 5, pp. 785-795 (1938).
 - [12] Hopkins, H. H. , : "On the diffraction theory of optical image" , Pro.Roy. Soc. A217, pp. 408-432 (1953).
 - [13] Y. Hirai, S. Tomida, K. Ikeda, M.Sasago, M. Endo, S. Hayama and N. Nomura , : "Three-Dimensional Resist Process Simulator PEACE" , IEEE Trans. Comput. Aided Des., vol. 10, No. 6, pp. 802-807 (1991).
 - [14] D. Adalsteinsson and J. A. Sethian , : "A Level Set Approach to a Unified Model for Etching, Deposition, and Lithography I : Algorithms and Two-Dimensional Simulations" , Journal of Computational Physics 120, pp. 128-144 (1995).
 - [15] Y. Sensu and A. Sekiguchi , : "Improved resolution of thick film resist" , SPIE, 4979, pp. 561-581 (Jan. 2003).
 - [16] Y. Sensu, A. Sekiguchi and Y. Miyake , : " Study on Improved Resolution of Thick Film Resist (Verification by Simulation) " , Advances in Resist Technology and Processing, Proc. SPIE, vol. 4345, pp. 921-935 (Feb. 2001).

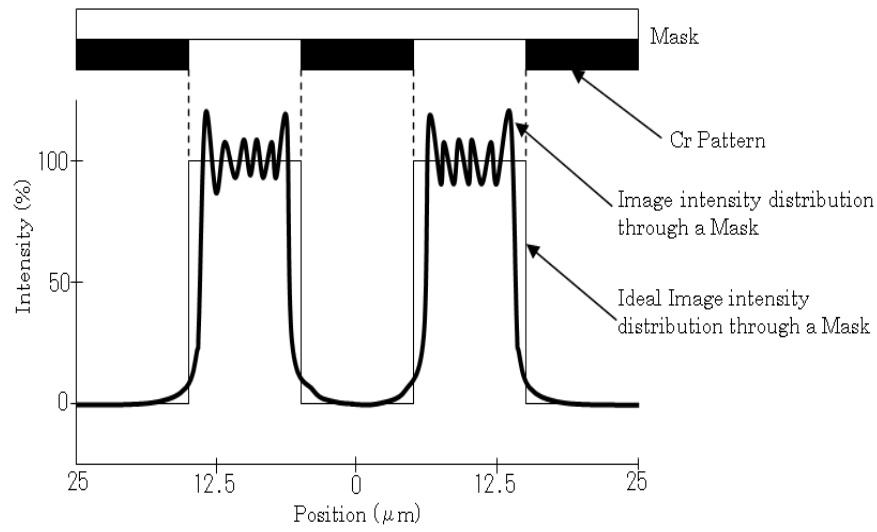


Fig.1 Schematic diagram of the distribution of light intensity on the resist surface.

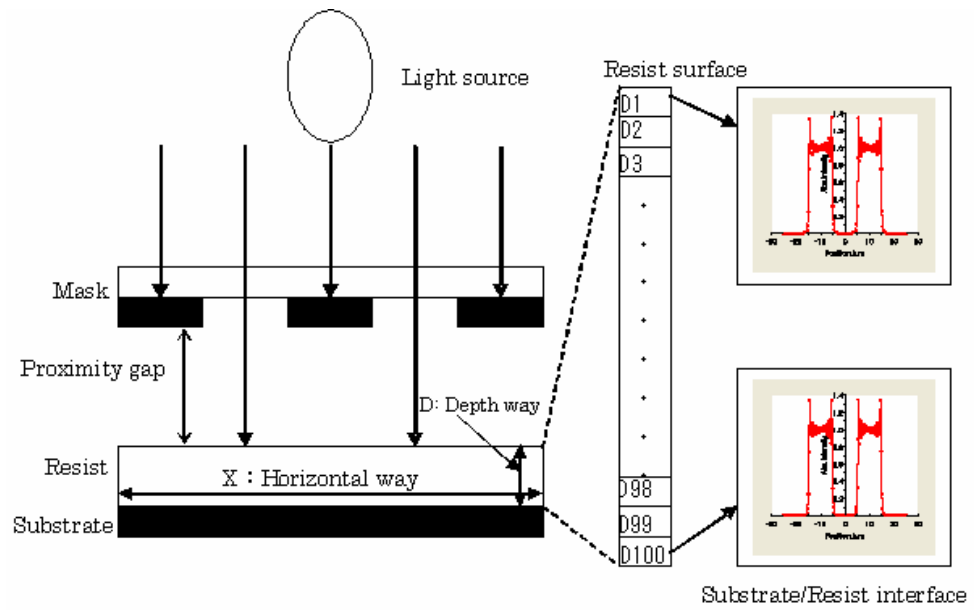


Fig.2 Schematic diagram of the light intensity distribution in the resist film.



Fig.3 Resist thickness measurement system.

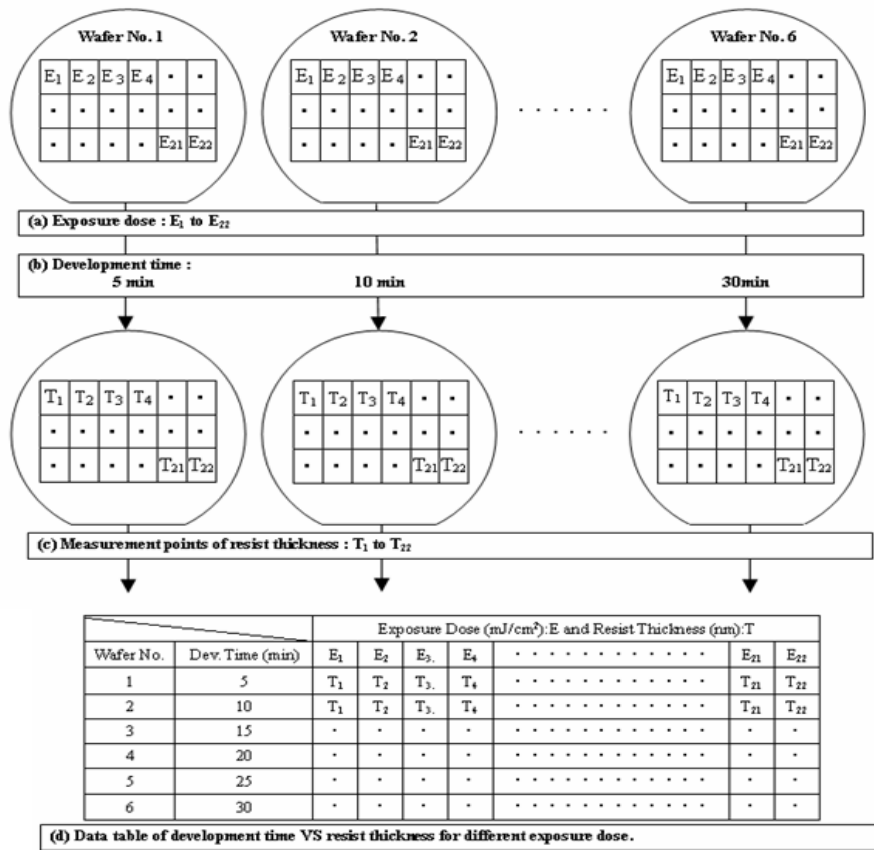


Fig.4. Measurement method of development rate.

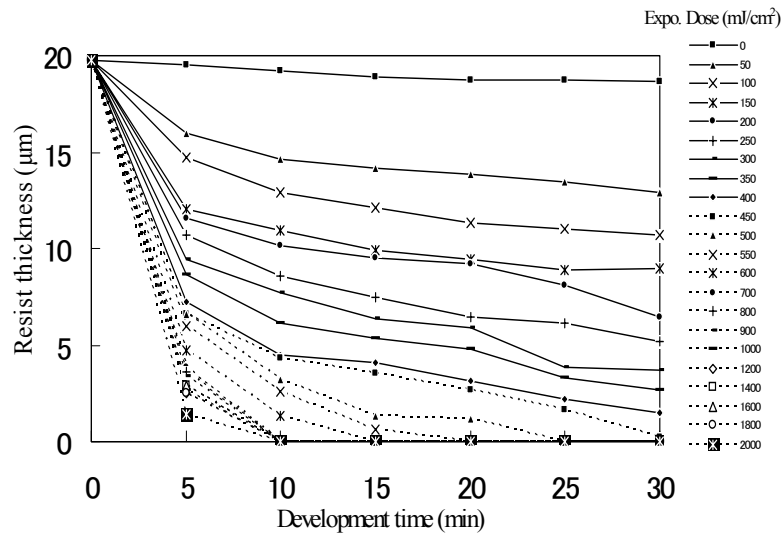


Fig.5 Measurement result of development time vs resist thickness.

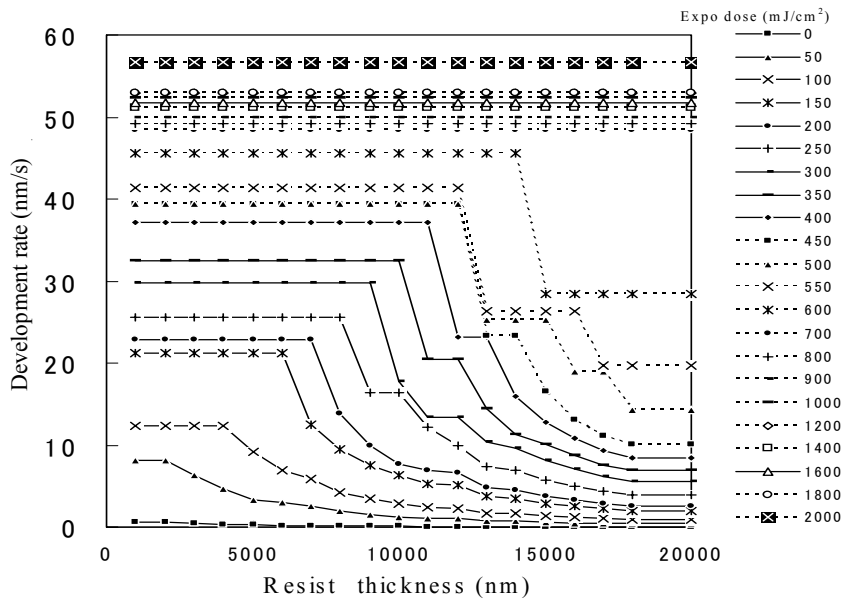
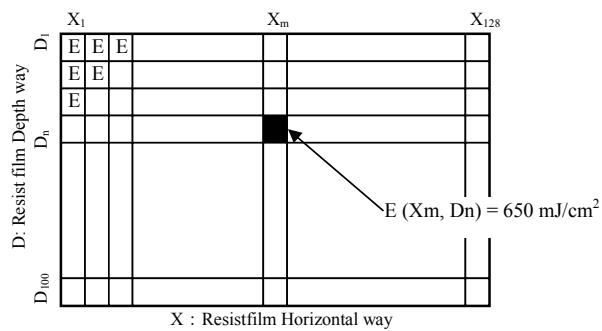
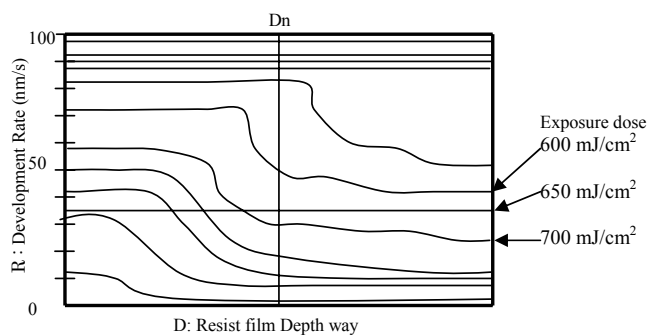


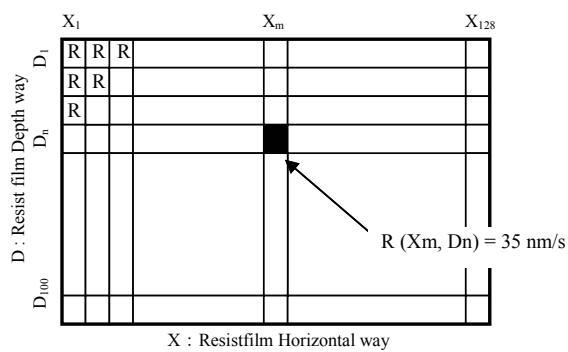
Fig.6 Development rate of in the resist film for the defferent exposure dose.



(a) Two-dimensional distribution of exposure dose in a resist film.



(b) Development rate distribution in a resist film.



(c) Two-dimensional distribution of development rate in a resist film.

Fig.7 Procedure for estimating two-dimension development rate distribution in a resist film.

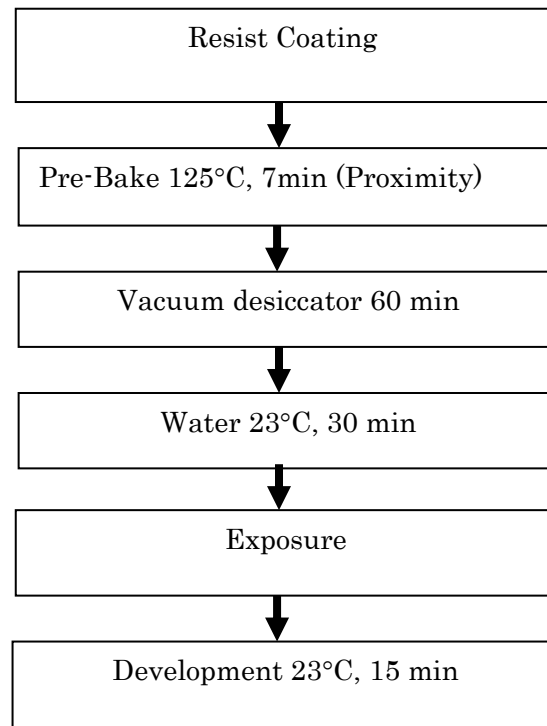


Fig.8 Experimental conditions and the process flow for the preparation of test samples.



Fig.9 Mask aligner of the proximity printing type.

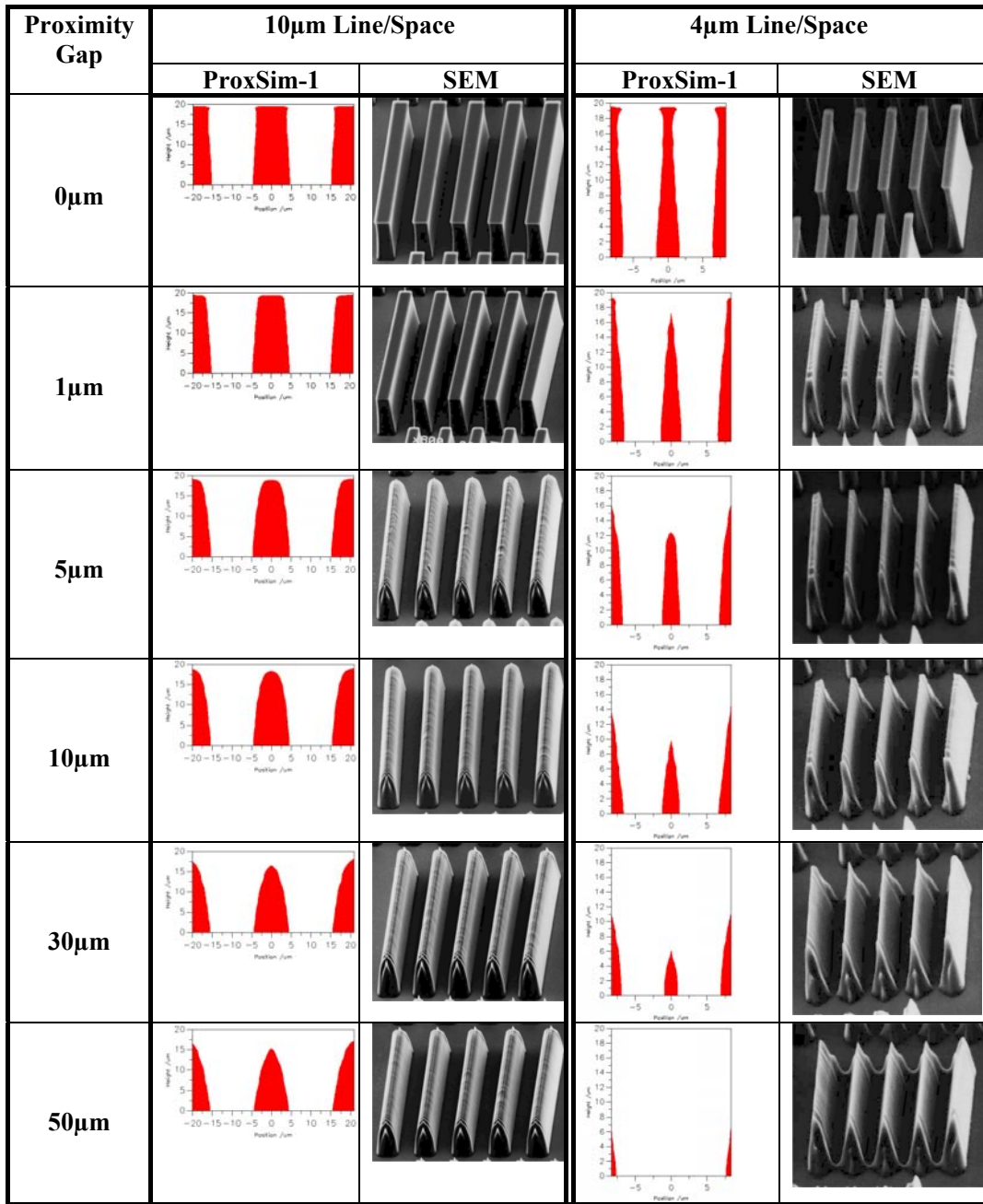


Fig.10 Results of SEM observation and of calculations using ProxSim-1.

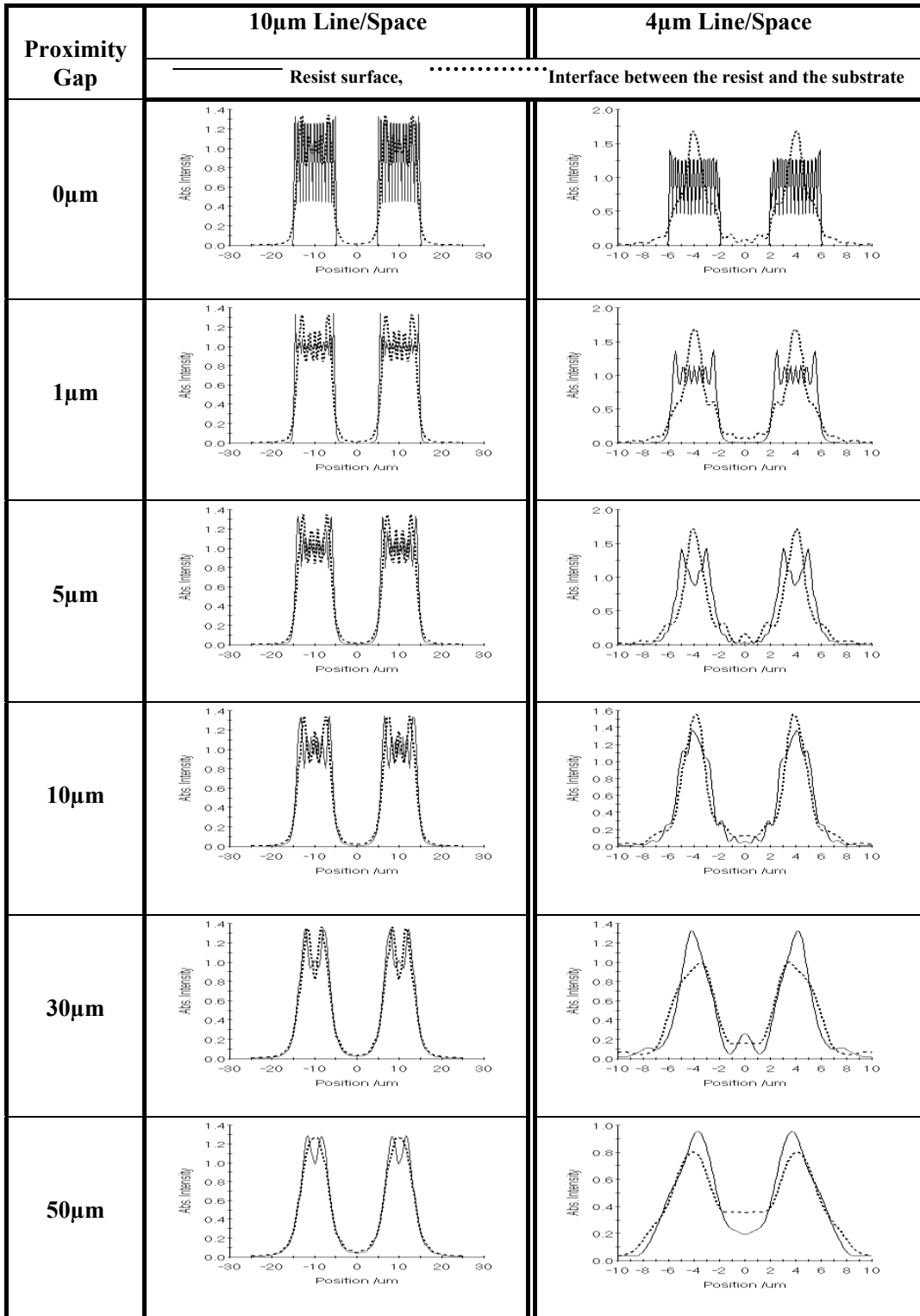


Fig.11 Results of calculations for light intensity at the resist surface and at the interface between the resist and the substrate.

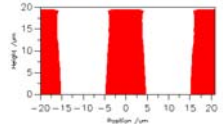
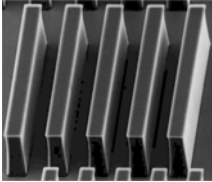
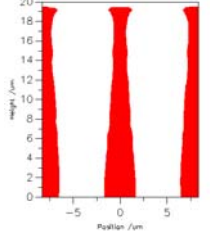
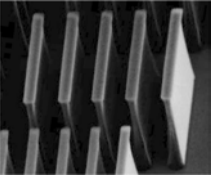
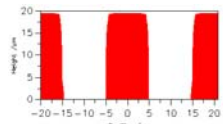
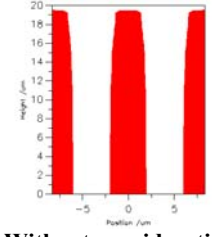
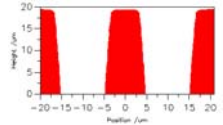
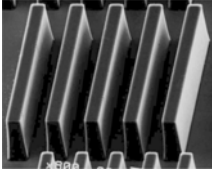
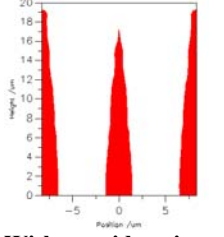
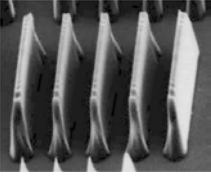
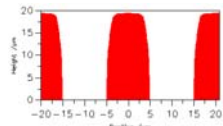
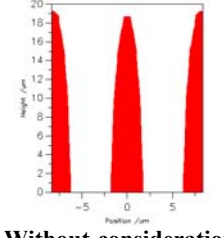
Proximity Gap	10 μ m Line/Space		4 μ m Line/Space	
	ProxSim-1	SEM	ProxSim-1	SEM
0 μ m	 <p>With consideration to the gap effect in the resist film.</p>		 <p>With consideration to the gap effect in the resist film.</p>	
	 <p>Without consideration to the gap effect in the resist film.</p>		 <p>Without consideration to the gap effect in the resist film.</p>	
1 μ m	 <p>With consideration to the gap effect in the resist film.</p>		 <p>With consideration to the gap effect in the resist film.</p>	
	 <p>Without consideration to the gap effect in the resist film.</p>		 <p>Without consideration to the gap effect in the resist film.</p>	

Fig.12 Comparison between the results of the resist profile simulation with and without consideration to the gap effect in the resist film.